Available online at www.sciencedirect.com
ScienceDirect
Trans. Nonferrous Met. Soc. China 22(2012) 2451−2458
Transactions of Nonferrous Metals Society of China
www.tnmsc.cn

Self-assembly of hierarchical $ZnSnO_3$−SnO_2 nanoflakes and their gas sensing properties

ZENG Yi, BING Yi-fei, LIU Chang, ZHENG Wei-tao, ZOU Guang-tian

State Key Laboratory of Superhard Materials; Key Laboratory of Automobile Materials, Ministry of Education; College of Materials Science and Engineering, Jilin University, Changchun 130012, China

Received 9 July 2012; accepted 6 August 2012

Abstract: A new type of hierarchical $ZnSnO_3$−SnO_2 flower-shaped nanostructure composed of thin nanoflakes as secondary units is successfully prepared through a simple hydrothermal process. The polyhedral $ZnSnO_3$ core acts as a sacrificed template for the growth of hierarchical SnO_2 nanoflakes, and the average thickness of SnO_2 nanoflakes is around 25 nm. The time-dependent morphology evolution of $ZnSnO_3$−SnO_2 samples was investigated, and a possible formation mechanism of these hierarchical structures is discussed. The gas sensor based on these novel $ZnSnO_3$−SnO_2 nanostructures exhibits high response and quick response-recovery traits to ethanol (C_2H_5OH). It is found that $ZnSnO_3$−SnO_2 nanoflakes have a response of 27.8 to 50×10^{-6} C_2H_5OH at the optimal operating temperature of 270 °C, and the response and recovery time are within 1.0 and 1.8 s, respectively.
Key words: complex nanostructure; hierarchical structure; hydrothermal synthesis; gas sensor

1 Introduction

Micro- or nano-sized functional materials with controlled shape and size have attracted large interest and exhibit a wide range of new potential applications, because it is well-known that the properties of materials depend not only on their composition, but also on their microstructure, phase, shape, and size [1−3]. In recent years, the design and assembly of nanosized building blocks (particles, rods, or sheets) to form complex and hierarchical architectures have attracted much attention [4−7]. To prepare these complex architectures, various physical methods such as thermal evaporation, chemical vapor deposition (CVD), and other gas-phase synthesis reaction have been employed successfully to assemble building blocks into different micro- or nano-structures. However, complex operating steps, sophisticated equipments, or high temperatures are involved in these gas-phase routes. Alternatively, solution-based routes including self-assembly and template-assisted process are attractive and developed due to their mild synthetic conditions and potential for scale-up.

Zinc stannate ($ZnSnO_3$), as a multifunctional material, has attracted considerable attention to the synthesis and various properties due to its extensive applications in various fields, such as gas sensors, moisture detectors, and electronics materials [8−10]. Up to now, several synthesis routes have been successfully employed for the preparation of different $ZnSnO_3$ micro- and nano-materials [9,11,12]. By the methods mentioned above, hydrothermal process may be one of the most promising routes, due to its low cost, and potential advantage for assembly of nanosized building blocks to form complex and hierarchical architectures. Currently, much effort has been exerted to realize basic low-dimensional $ZnSnO_3$ nanostructures (nano-particles, -rods, or -wires), and few literatures are related to the synthesis and applications of hierarchical $ZnSnO_3$ nanoarchitectures or $ZnSnO_3$/oxides nanocomposites. Furthermore, one-step hydrothermal synthesis and gas-sensing properties for the hierarchical $ZnSnO_3$−SnO_2 nanostructures assembled from 2D nanoflakes as building blocks have not been reported.

Previously, we have presented a low-cost and simple hydrothermal process for the synthesis of $ZnSnO_3$ nanocages and nanoskeletons, hierarchical nanocages and microspheres [13−15]. Here, we firstly use the

Foundation item: Projects (50832001, 51002014) supported by the National Natural Science Foundation of China; Project (20110491319) supported by China Postdoctoral Science Foundation
Corresponding author: ZHENG Wei-tao; Tel: +86-431-85168246; E-mail: wtzheng@jlu.edu.cn
DOI: 10.1016/S1003-6326(11)61484-2

improved hydrothermal route to fabricate hierarchical $ZnSnO_3$−SnO_2 nanoflakes and investigate their gas-sensing performance. The crystallinity, morphology, and crystal structure of the as-prepared sample have been characterized. Moreover, the formation process has been investigated through the morphology evolution with the reaction time, and a possible formation mechanism is proposed. Excellent ethanol sensing properties with quick response and recovery time based on hierarchical $ZnSnO_3$−SnO_2 nanoflakes have been obtained.

2 Experimental

2.1 Synthesis and characterization of $ZnSnO_3$−SnO_2

Hierarchical $ZnSnO_3$−SnO_2 nanoflakes were prepared through a facile one-step hydrothermal process. Zinc oxide (ZnO), tin tetrachloride ($SnCl_4·5H_2O$), cetyltrimethyl ammonium bromide (CTAB), and sodium hydroxide (NaOH) were purchased from Beijing Chemical Reagent Co. Ltd. and used as-received without further purification. Briefly, a 40 mL of aqueous solution of ZnO (3.0 mmol) and $SnCl_4·5H_2O$ (7.0 mmol) was mixed with vigorous agitation at room temperature for 10 min, then mixed solution of 0.02 mol/L CTAB and 0.16 mol/L NaOH was dropped into the mixture solution with stirring for 10 min to form a uniform suspension. The suspension was transferred to a Teflon-lined stainless steel autoclave, sealed tightly, and maintained at 180 °C for 12 h. After the autoclave was cooled naturally down to room temperature, the collected precipitates were washed several times with absolute ethanol and deionized water, and dried at 90 °C in air to get the final products.

The phase purity, morphology, and structure of the obtained products were characterized by X-ray powder diffraction (XRD, Rigaku D/max-2500, Cu K_α, λ= 0.15418 nm), field emission scanning electron microscopy (FESEM, JEOL JSM−6700F, operated at 8 kV) with attachment of energy dispersive X-ray spectrometry (EDX), transmission electron microscopy (TEM, Hitachi H−8100, 200 kV), and high-resolution TEM (HRTEM, JEOL−2100F, 200 kV), respectively.

2.2 Fabrication and measurement of $ZnSnO_3$−SnO_2 sensor

The gas-sensing properties of $ZnSnO_3$−SnO_2 were measured with a WS−60A gas-sensing characterization system (Weisheng Instruments Co. Ltd., China). The fabrication process of the gas sensor was briefly described: the as-synthesized sample was mixed with water and then coated on a ceramic tube on which two platinum wires had been installed at each end. To keep the sensor working at a elevated temperature, a Ni–Cr alloy coil was inserted into the ceramic tube as a heater. The detailed fabrication process of the gas sensor based on the as-prepared sample had been described in elsewhere [16,17]. The desired concentrations of the testing gases were obtained by the static liquid gas distribution method, which was calculated by the following formula [18]:

$$V_Q=(V\varphi M)/(22.4d\rho)\times10^{-9}\times(273+T_R)/(273+T_B) \quad (1)$$

where V_Q is the liquid volume of the volatile compound; V is the volume of the testing chamber; φ is the required gas volume fraction; M is the relative molecular mass; ρ is the mass density; d is the purity of the volatile testing liquid; T_R and T_B are the temperatures at the ambient and test chamber, respectively. The response (R) of the sensor was defined as the ratio (R_a/R_g) of the resistance of the sensor in dry air (R_a) to that in the testing gas (R_g). The response and recovery time were defined as the time taken by the sensor to achieve 90% of the total resistance change in the case of adsorption and desorption, respectively.

3 Results and discussion

3.1 Structural and morphological characteristics

XRD characterization is used to investigate the crystal structures of the as-prepared products, which is shown in Fig. 1. The crystal phase of the products consists of mixed oxides, including $ZnSnO_3$ and SnO_2. One part of all diffraction peaks (solid pattern) can be well matched to the standard diffraction pattern of perovskite $ZnSnO_3$ structure from the Joint Committee on Powder Diffraction Standards card (JCPDS No. 11-0274), and the residual diffraction peaks are indexed to the tetragonal rutile structure of SnO_2 (JCPDS No. 41-1445). No diffraction peaks from any other impurity are detected, demonstrating that the as-prepared products are only composed of $ZnSnO_3$ and SnO_2.

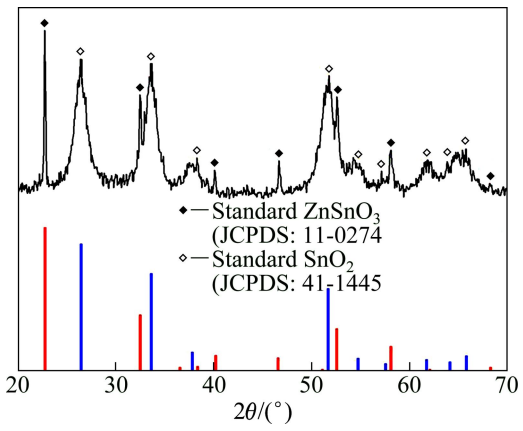

Fig. 1 XRD patterns of as-prepared product and standard $ZnSnO_3$ (JCPDS No. 11-0274) and SnO_2 (JCPDS No. 41-1445)

The morphological and microstructures of the as-prepared $ZnSnO_3$−SnO_2 products were characterized by FESEM and TEM observations. From a panoramic FESEM image (Fig. 2(a)), the as-prepared products contain numerous flowerlike aggregates with multi-leaves. It can be seen clearly that the flowerlike aggregates show analogous morphology and ellipsoid profile with the horizontal axis of approximate 1.9 μm and longitudinal axis of 1.2 μm. Increasing the magnification (Fig. 2(b)), it is possible to observe that a single flowerlike aggregate with a hierarchical structure is composed of many thin nanoflakes, arraying in different directions extending radially from a common central zone. The individual nanostructure usually exhibits a hierarchical structure with various sized and shaped nanoflakes as secondary units. At high magnification (Fig. 2(c)), careful information has been achieved by the measure of the thickness perpendicular to its 2D surface, revealing that a representative nanoflake is about 25 nm in thickness. The low-magnification TEM image of the sample after a long time sonication in ethanol is shown in Fig. 2(d). It can be observed that the unshaped cross-sections detected from the horizontally dispersed flakes are in good agreement with the above FESEM observations, and the vertically aligned flakes appear to have a rod-like morphology. The representative HRTEM image is displayed in Fig. 2(e), which was taken with electron beam perpendicular to the edge region of a flake. However, surprisingly, the lattice fringes in the HRTEM image confirm the single crystal nature of SnO_2 nanoflakes. The spacing between adjacent lattice planes is 0.336 nm, corresponding to (110) plane of rutile SnO_2. The two-dimensional fast Fourier transform (FFT) pattern belongs to rutile SnO_2 along the $[1\bar{1}\bar{1}]$ zone axis, which also indicates that the as-prepared nanoflakes have single-crystalline SnO_2 structure.

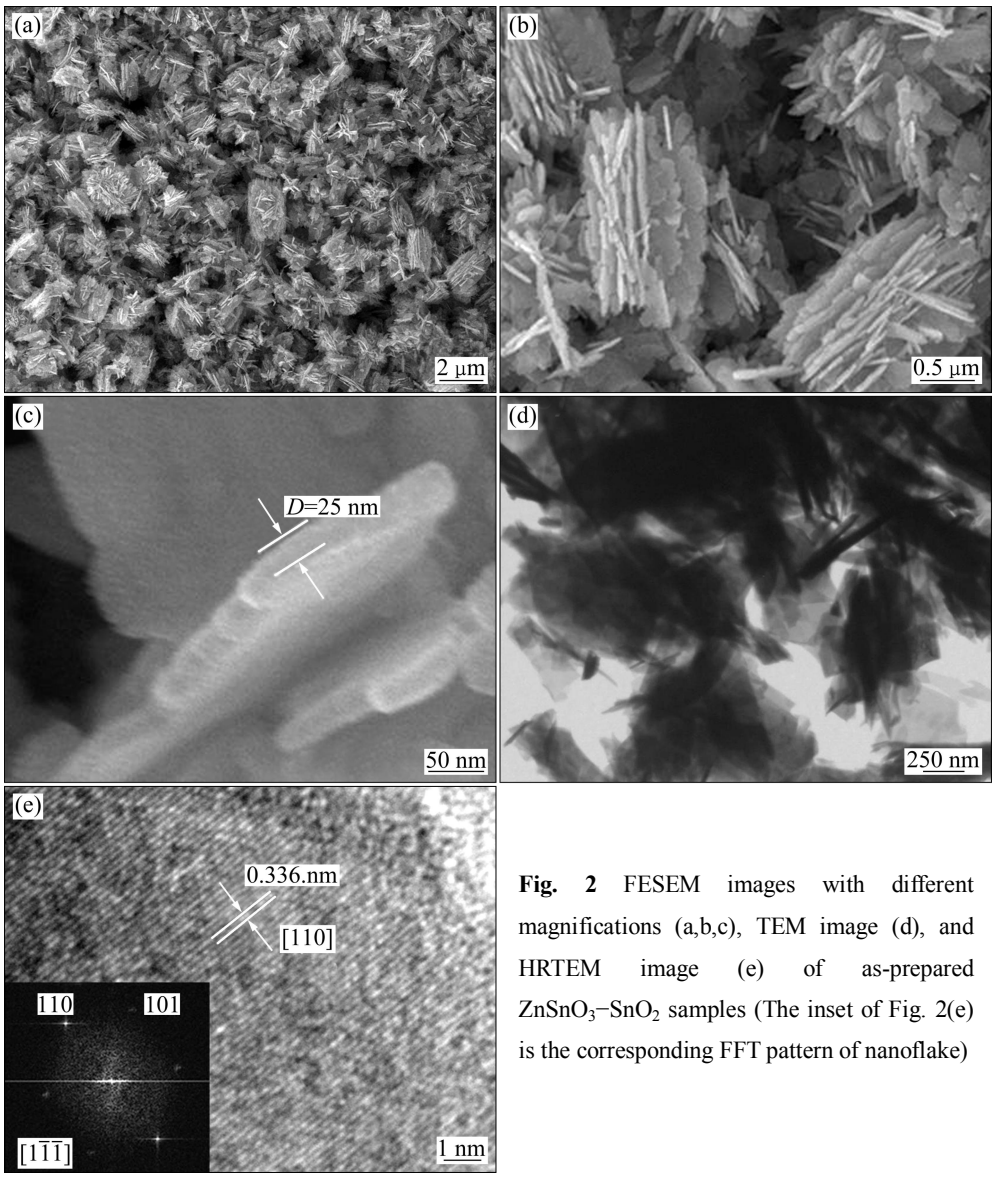

Fig. 2 FESEM images with different magnifications (a,b,c), TEM image (d), and HRTEM image (e) of as-prepared $ZnSnO_3$−SnO_2 samples (The inset of Fig. 2(e) is the corresponding FFT pattern of nanoflake)

3.2 Growth process and mechanism

To understand how these self-assembly nanostructures are formed, we have also investigated the morphological evolution of the samples obtained at different reaction time, as shown in Figs. 3(a−d). It is demonstrated that the shape and size of the hierarchical nanostructures can be actively controlled by adjusting the reaction time. When the reaction time is 30 min, as shown in Fig. 3(a), it can be observed that the sample just consists of many irregular polyhedra with some floccules on the corners. XRD pattern of this sample confirms that all of the diffraction peaks are well matched with the $ZnSn(OH)_6$, indicating that the metastable $ZnSn(OH)_6$ intermediate phase is formed at early stage [13]. When the reaction time was prolonged to 4 h, the irregular $ZnSn(OH)_6$ polyhedra and nanorod-assembled SnO_2 floccules coexist (Fig. 3(b)), but it is observed that all polyhedra surfaces are almost covered by nanorod-assembled SnO_2 floccules. Increasing the reaction time up to 8 h, no polyhedra is observed and the floccules transform into the flowerlike aggregates with coarse surfaces (Fig. 3(c)). When the reaction time increases to 12 h, the hierarchical nanoflakes are formed, of which detailed characteristics have been discussed in the above section. Further extending the reaction time up to 20 h (Fig. 3(d)), the flowerlike architecture gradually transforms into thick nanosheets and fragments.

On the basis of the experimental results and the investigations described above, the formation of hierarchical $ZnSnO_3$−SnO_2 nanoflakes probably involves three key steps, which are schematically illustrated in Fig. 3(e). In the first step, the presence of Zn^{2+} and Sn^{4+} is easy to form $ZnSn(OH)_6$ nuclei in the alkaline solution. Subsequently, in hydrothermal process, it occurs quickly for the self-assembly of the nuclei to form polyhedral-shaped $ZnSn(OH)_6$ crystals since the aggregated process is structurally and energetically favorable. Then, the secondary nucleation of excessive SnO_2 occurs on the corners and inevitable defects on the surfaces of $ZnSn(OH)_6$ polyhedra, followed by subsequent growth of the nanorod-assembled SnO_2 floccules. The size reduction and the final disappearance of $ZnSn(OH)_6$ polyhedra may be due to the fact that the nanorods coalesce and the dissolution-recrystallization process happens in this stage. Finally, the $ZnSn(OH)_6$ intermediate phase not only acts as the sacrifice template for the assembly of hierarchical SnO_2 nanoflakes, but also is decomposed and recrystallized to transform into $ZnSnO_3$ phase according to a selective dissolution-recrystallization followed by Ostwald ripening under hydrothermal conditions [19].

3.3 Gas-sensing properties and mechanism

Firstly, it is well-known that the response of the gas sensor is greatly influenced by the operating temperature and exhibits a peak value at a certain operating temperature. The maximum response is obtained at the so-called optimal operating temperature, which retains the equilibration of the diffusion of the gas molecules compensated to the surface and the reaction of the testing gas molecules with the adsorbed oxygen species [20]. In order to obtain the optimal operating temperature, the response of the sensor to 100×10^{-6} ethanol at the operating temperature in the range of 170−350 °C have been tested, as shown in Fig. 4. It shows that the response of the $ZnSnO_3$−SnO_2 sensor towards ethanol increases and reaches the maximum at the operating temperature of 270 °C, and then decreases with further increasing the temperature. The optimal operating temperature of 270 °C is applied to all the investigations hereinafter.

Figure 5 shows the dependence of response as a function of ethanol concentration for the $ZnSnO_3$−SnO_2 sensor. It can be observed that the sensor has a wide detection range to ethanol from 5 to 5000×10^{-6}. The response rapidly increases with increasing ethanol concentration below 200×10^{-6}. Above 200×10^{-6}, the

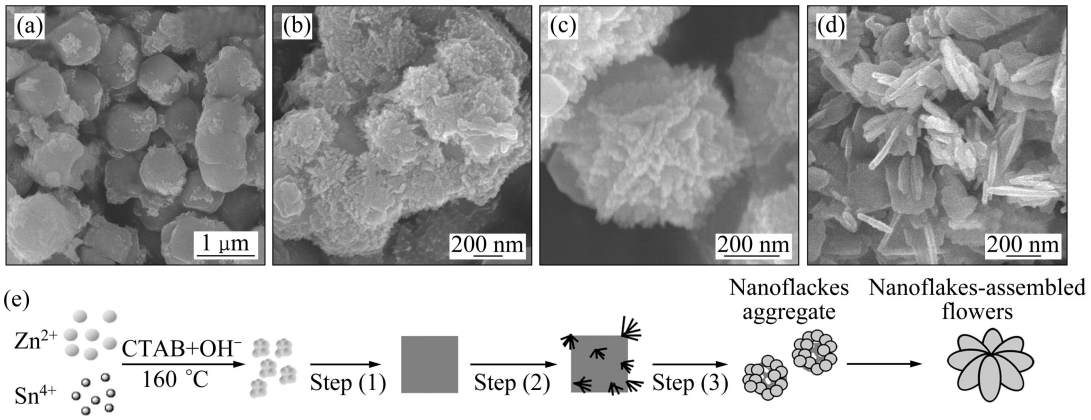

Fig. 3 FESEM images showing morphology evolution of samples obtained at different reaction time of 30 min (a), 4 h (b), 8 h (c) and 20 h (d) and schematic illustration of possible formation process of $ZnSnO_3$−SnO_2 nanoflakes (e)

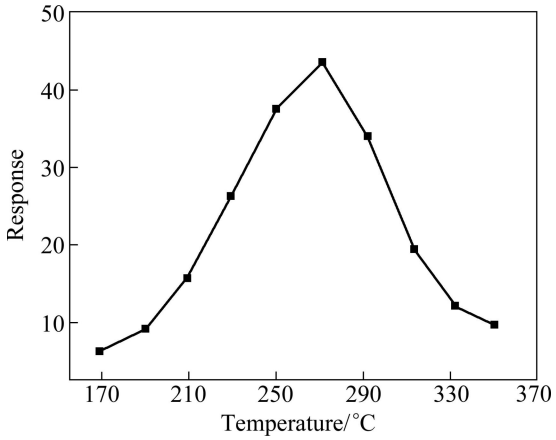

Fig. 4 Response of sensor versus operating temperature to 100×10^{-6} ethanol

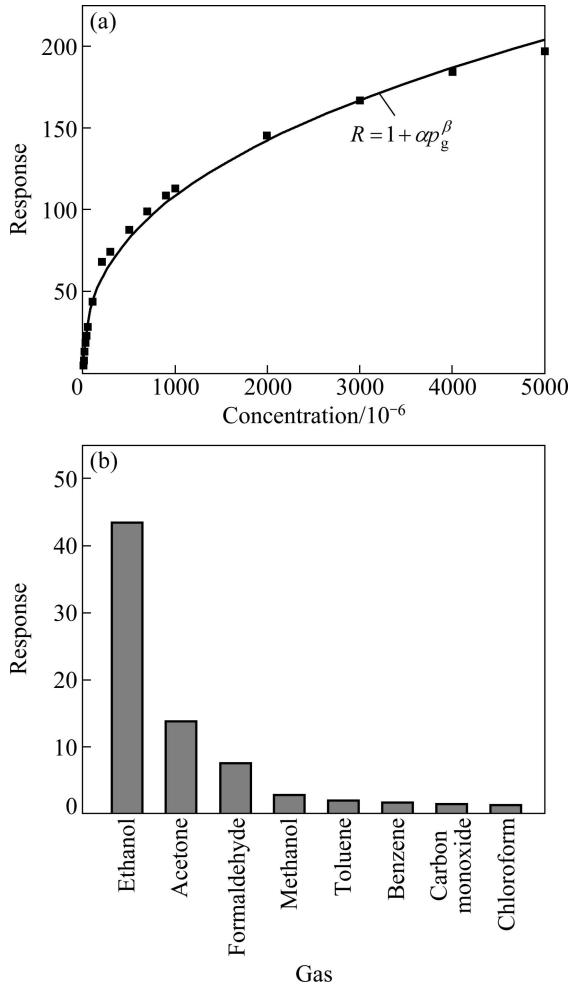

Fig. 5 Response transients of sensor versus ethanol concentration at 270 °C (a) and selectivity of sensor to different testing gases (b)

sensor response increases less rapidly with the increasing ethanol concentration. When the ethanol concentration is in the range of $(4000-5000)\times10^{-6}$, the response increase slows down, indicating that the sensor becomes more or less saturated. In fact, the relationship between the response and the testing gas concentration can be described by an empirical equation as: $R=1+\alpha p_g^{\beta}$ [21,22], where R is response; p_g is the partial pressure of the testing gas, which is proportional to the concentration of the testing gas; α and β are constants, and β actually is always in the range of 0.5−1, which is derived from the surface interaction process. For our nanostructures, β is fitted to $\beta=0.397\pm0.016$, and the deviation from the ideal value is probably due to the agglomeration of nanostructures during the testing process at high operating temperature or less sensitive areas existing in the sample [23]. As shown in Fig. 5(b), the gas responses of the sensor based on the hierarchical $ZnSnO_3$−SnO_2 nanoflakes were tested at the operating temperature of 270 °C to various testing gases (100×10^{-6}), such as ethanol, acetone and formaldehyde (HCHO). Hierarchical $ZnSnO_3$−SnO_2 nanoflakes exhibit an obvious response to C_2H_5OH, little response to acetone and HCHO, and almost insensitive to methanol, toluene, benzene, carbon monoxide, and chloroform. The highest response of the sensor to ethanol is about 43.6, while the responses to other gases are no greater than 14. It is obvious that the selectivity of the sensor based on $ZnSnO_3$−SnO_2 nanoflakes to ethanol against other gases exceeds almost by 3 times. It is concluded that the gas sensor has satisfactory selectivity to ethanol.

Figure 6 shows the response transient of the sensor to 20×10^{-6} ethanol at the optimal operating temperature of 270 °C, which indicates that our sensor has a fast response-recovery process. It is found that the response of the hierarchical nanostructures is about 13.5×10^{-6} to 20×10^{-6} ethanol. The response time and recovery time are about within 1.0 and 1.8 s, respectively. Figure 6(b) shows three sequential cycles of response transients of the gas sensor to 20×10^{-6} ethanol at this temperature, indicating a reversible, repeatable yet stable characteristic.

The response and recovery behaviors of the gas sensor being orderly exposed to different concentrations of ethanol were also investigated, as shown in Fig. 7. In the measurements, the responses are about 4.1, 7.8, 18.4, 22.6, and 27.8 to 5×10^{-6}, 10×10^{-6}, 30×10^{-6}, 40×10^{-6}, and 50×10^{-6} ethanol, respectively. The signal from the sensor based on the nanostructures becomes stable and returns to the original value within 1.8 s after the tested gas was replaced by ambient atmosphere. Compared with our previous reported on the sensing properties of pure $ZnSnO_3$ nanostructures [13,14], the $ZnSnO_3$−SnO_2 nanoflakes with hierarchical structure exhibit a significantly improved recovery behavior, which can be ascribed to the framework of oxygen molecules diffusing

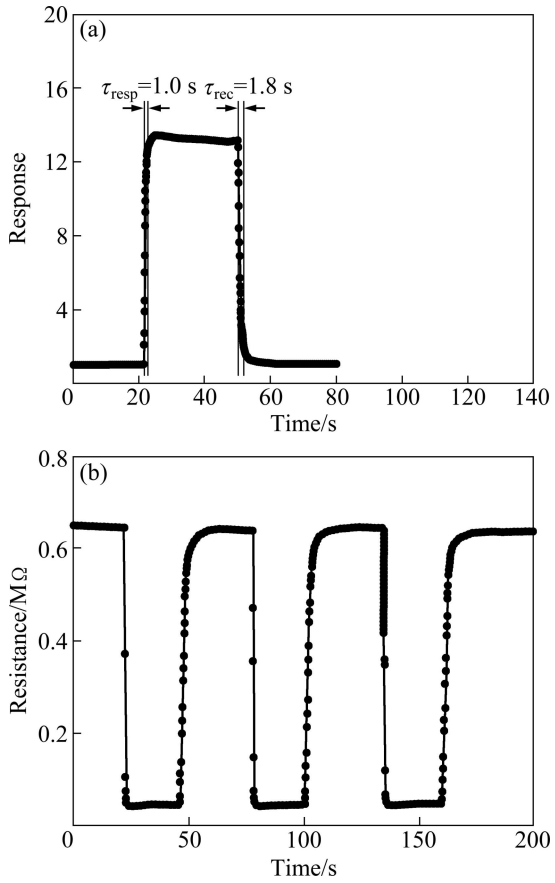

Fig. 6 Response transients of sensor to 20×10^{-6} ethanol (a) and three periods of response curve (b)

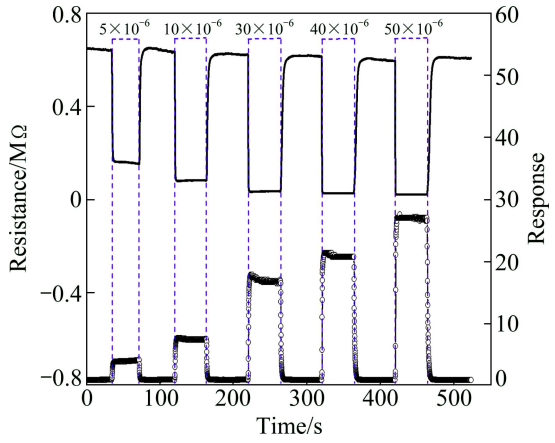

Fig. 7 Response transients of sensor to different concentrations of ethanol

toward the materials surface. Actually, the surface-controlled sensing process involves the adsorption and desorption process occurring on the surface of sensing materials [20]. The efficient utilization of the high surface area and surface accessibility are crucial to maintaining the high and fast response of nanocrystals, whereas the recovery characteristic is decided by the framework of the gas diffusion toward the sensing surface, the reaction with chemisorbed oxygen ions, and the subsequent re-oxidation process of the sensing surface to yield oxygen species [24]. Surface accessibility should be considered to be the key factor that determines the recovery characteristic. According to LEE [24], plenty of nanoflakes with hierarchical architecture can provide various micro- and nano-porosity for effective gas diffusion and surface accessibility, which may lead to the fast recovery process.

It is believed that the sensitive mechanism for the response and recovery processes probably involves some key reactions: adsorption, oxidation, and desorption, resulting in the resistance change of the semiconductor sensing materials [25,26]. When $ZnSnO_3$−SnO_2 nanoflakes are exposed to air, oxygen molecules can be chemisorbed on the surface to form O_2^-, O^-, or O^{2-} ions by capturing electrons from the conduction band, which in turn produces an electron depletion layer at the surface region of the nanoflakes. When the adsorption process arrives certain equilibrium, the sensor shows a higher resistance. Subsequently, when reductive gas such as ethanol is introduced at the moderate temperature, the surface of these nanoflakes is exposed to the traces of reductive gas. The interaction between ethanol molecules and chemisorbed oxygen ions reduces the concentration of oxygen ions on the nanoflake surface, by which the free electrons are released and the electron concentration thus increases. As a result, the conductivity of the gas sensor eventually increases.

$$C_2H_5OH(g)\rightarrow C_2H_5OH(ad) \quad (2)$$

$$2C_2H_5OH\ (ad)+4O^{2-}(ad)\rightarrow 2C_2H_4O^-(ad)+O_2(g)+2H_2O+6e^- \quad (3)$$

Furthermore, Table 1 lists a comparison of the crystallographic composition and ethanol sensing performance of our $ZnSnO_3$−SnO_2 samples prepared with different reaction time with other pure $ZnSnO_3$- and SnO_2-based sensors. Note that the recovery time is more than 25 s for $ZnSnO_3$ sensor to 100×10^{-6} ethanol. In contrast, the recovery time of the $ZnSnO_3$−SnO_2 samples prepared with different reaction time of 8, 12, and 20 h is about 8, 1.8, and 4 s, respectively. These results suggest that the SnO_2 phase plays a more important role in the fast recovery characteristic to ethanol than $ZnSnO_3$. On the other hand, it also shows that the response of our samples towards ethanol increases and reaches the maximum at the reaction time of 12 h, and then decreases with further increasing the reaction time. Thus, the improved sensing performance may be attributed to the rational hierarchical architectures and the coexisted SnO_2 phases, which can enhance both the gas response and the response speed simultaneously and substantially.

Table 1 Comparison of ethanol sensing properties of $ZnSnO_3$ and SnO_2 samples in literatures with our samples obtained with different reaction time at corresponding operating temperature

Ref.	Reaction time/h	Crystallographic composition/%		Response	Time/s	
		$ZnSnO_3$	SnO_2		Response	Recovery
[13]		100	0	13.4	2	30
[14]		100	0	13.1	2	30
This work	0.5	100	0	10.1	2	25
	8	74	26	25.4	1.5	8
	12	48	52	43.6	1	1.8
	20	21	79	32.8	2	4
[27]		0	100	33.1(50×10^{-6})	1	1−2[a]
[28]		0	100	48.38	8	6−8[a]

a: The corresponding recovery time is not listed, and the listed data are estimated from the original literatures.

4 Conclusions

1) Flowerlike $ZnSnO_3$−SnO_2 nanoflakes with hierarchical structure assembled from 2D SnO_2 nanoflakes as building blocks, exhibiting porous, and an easy penetrability and surface accessibility, can be obtained through a facile hydrothermal process.

2) The time-dependent morphology evolution confirms that the polyhedral $ZnSnO_3$ core acts as a sacrificed template for the growth of hierarchical SnO_2 nanoflakes.

3) Gas sensor based on hierarchical $ZnSnO_3$−SnO_2 nanostructures has good gas sensing performance for detecting ethanol gas, and the response and recovery time of this sensor are within 1.0 and 1.8 s, respectively.

References

[1] PENN R L, BANFIELD J F. Imperfect oriented attachment: Dislocation generation in defect-free nanocrystals [J]. Science, 1998, 281: 969−971.

[2] GAO P X, WANG Z L. Mesoporous polyhedral cages and shells formed by textured self-assembly of ZnO nanocrystals [J]. J Am Chem Soc, 2003, 125: 11299−11305.

[3] GENG L N. Gas sensitivity of polyaniline/SnO_2 hybrids to volatile organic compounds [J]. Transactions of Nonferrous Metals Society of China, 2009, 19(s): s678−s683.

[4] SHIMIZU Y, JONO A, HYODO T, EGASHIRA M. Preparation of large mesoporous SnO_2 powders for gas sensor applications [J]. Sens Actuators B, 2005, 108: 56−61.

[5] LOU X W, ARCHER L A, YANG Z. Hollow micro-/nanostructures: synthesis and applications [J]. Adv Mater, 2008, 20: 3987−4019.

[6] ZHANG H, WU J, ZHAI C, DU N, MA X, YANG D. From ZnO nanorods to 3D hollow microhemispheres: solvothermal synthesis, photoluminescence and gas sensor properties [J]. Nanotechnology, 2007, 18: 455604.

[7] JIAO W L, ZHANG L. Preparation and gas sensing properties for acetone of amorphous Ag modified $NiFe_2O_4$ sensor [J]. Transactions of Nonferrous Metals Society of China, 2012, 22: 1127−1132.

[8] WANG Z C, LIU T M, YU L. Preparation and properties of ultra-purity and nanosized $ZnSnO_3$ gas sensitive material [J]. J Chin Ceram Soc, 2004, 32: 1555−1559.

[9] SHEN Y S, ZHANG T S. Preparation, structure and gas-sensing properties of ultramicro $ZnSnO_3$ powder [J]. Sens Actuators B, 1993, 12(1): 5−9.

[10] ZHANG T S, SHEN Y S, ZHANG R F. Ilmenite structure-type β-$CdSnO_3$ used as an ethanol sensing material [J]. Mater Lett, 1995, 23: 69−71.

[11] XUE X Y, CHEN Y J, LI Q H, WANG C, WANG Y G, WANG T H. Electronic transport characteristics through individual $ZnSnO_3$ nanowires [J]. Appl Phys Lett, 2006, 88: 182102.

[12] KOVACHEVA D, PETROV K. Preparation of crystalline $ZnSnO_3$ from Li_2SnO_3 by low-temperature ion exchange [J]. Solid State Ionics, 1998, 9: 327−332.

[13] ZENG Y, ZHANG T, FAN H T, FU W Y, LU G Y, SUI Y M, YANG H B. One-pot synthesis and gas-sensing properties of hierarchical $ZnSnO_3$ nanocages [J]. J Phys Chem C, 2009, 113: 19000−19004.

[14] ZENG Y, ZHANG T, FAN H T, LU G Y, KANG M H. Synthesis and gas-sensing properties of $ZnSnO_3$ cubic nanocages and nanoskeletons [J]. Sens Actuators B, 2009, 143(1): 449−453.

[15] FAN H T, ZENG Y, XU X J, LV N, ZHANG T. Hydrothermal synthesis of hollow $ZnSnO_3$ microspheres and sensing properties toward butane [J]. Sens Actuators B, 2011, 153(1): 170−175.

[16] GE J P, WANG J, ZHANG H X, WANG X, PENG Q, LI Y D. High ethanol sensitive SnO_2 microspheres [J]. Sens Actuators B, 2006, 113(2): 937−943.

[17] ZENG Y, ZHANG T, WANG L J, KANG M H, FAN H T, WANG R, HE Y. Enhanced toluene sensing characteristics of TiO_2-doped flowerlike ZnO nanostructures [J]. Sens Actuators B, 2009, 140(1): 73−78.

[18] FAN H T, ZENG Y, YANG H B, ZHENG X J, LIU L, ZHANG T. Preparation and gas sensitive properties of ZnO−CuO nanocomposites [J]. Acta Phys –Chim Sin, 2008, 24: 1292−1296.

[19] YU S H, CÖLFEN H, ANTONIETTI M. Polymer-controlled morphosynthesis and mineralization of metal carbonate superstructures [J]. J Phys Chem B, 2003, 107: 7396−7405.

[20] YAMAZOE N, SAKAI G, SHIMANOE K. Oxide semiconductor gas sensors [J]. Catal Surv Asia, 2003, 7(1): 63−75.

[21] CHEN Y J, XUE X Y, WANG Y G, WANG T H. Synthesis and ethanol sensing characteristics of single crystalline SnO_2 nanorods [J]. Appl Phys Lett, 2005, 87: 233503.

[22] KIM I D, ROTHSCHILD A, HYODO T, TULLER H L. Microsphere templating as means of enhancing surface activity and gas sensitivity of $CaCu_3Ti_4O_{12}$ thin films [J]. Nano Lett, 2006, 6(2): 193−198.

[23] WILLIAMS D E. Semiconducting oxides as gas-sensitive resistors [J]. Sens Actuators B, 1999, 57(1−3): 1−16.

[24] LEE J H. Gas sensors using hierarchical and hollow oxide nanostructures: overview [J]. Sens Actuators B, 2009, 140(1): 319−336.

[25] XU M H, CAI F S, YIN J, YUAN Z H, BIE L J. Facile synthesis of highly ethanol-sensitive SnO_2 nanosheets using homogeneous precipitation method [J]. Sens Actuators B, 2010, 145(2): 875−878.
[26] FENG P, WAN Q, WANG T H. Contact-controlled sensing properties of flowerlike ZnO nanostructures [J]. Appl Phys Lett, 2005, 87: 213111.
[27] HYODO T, NISHIDA N, SHIMIZU Y, EGASHIRA M. Preparation and gas-sensing properties of thermally stable mesoporous SnO_2 [J]. Sens Actuators B, 2002, 83: 209−215.
[28] MAEKAWA T, TAMAKI J, MIURA N, YAMAZOE N. Development of SnO_2-based ethanol gas sensor [J]. Sens Actuators B, 1992, 9(1): 63−69.

$ZnSnO_3$−SnO_2 纳米片分级结构的自组装及气敏特性

曾 毅，邴一飞，刘 畅，郑伟涛，邹广田

吉林大学 材料科学与工程学院，汽车材料教育部重点实验室，超硬材料国家重点实验室，长春 130012

摘 要：通过一个简单的水热方法成功地合成出由 SnO_2 纳米片作次级结构的新型花状 $ZnSnO_3$−SnO_2 分级纳米结构。$ZnSnO_3$ 多面体在生长分级 SnO_2 纳米片的过程中主要起模版作用，制备出的 SnO_2 纳米片的厚度约为 25 nm。还讨论了 $ZnSnO_3$−SnO_2 样品的形貌随反应时间变化的规律，并且进一步讨论了形成这种分级结构的形成机制。此外，由这种新型 $ZnSnO_3$−SnO_2 纳米结构作敏感材料的气体传感器对乙醇气体具有高灵敏和快响应的特点。$ZnSnO_3$−SnO_2 纳米片在最佳工作温度 270 °C 时，对 50×10^{-6} 乙醇气体的灵敏度约为 27.8，其响应和恢复时间分别在 1 s 和 1.8 s 内。

关键词：复合纳米结构；分级结构；水热合成；气体传感器

(Edited by YANG Hua)